Acetonitrile Transition Metal Interfaces from First Principles

Ludwig, Thomas; Singh, Aayush R.; Nørskov, Jens K.

Published in:
Journal of Physical Chemistry Letters

Link to article, DOI:
10.1021/acs.jpclett.0c02692

Publication date:
2020

Document Version
Peer reviewed version

Acetonitrile Transition Metal Interfaces from First Principles

Thomas Ludwig, Aayush R. Singh, and Jens K. Nørskov*

ABSTRACT: Acetonitrile is among the most commonly used nonaqueous solvents in catalysis and electrochemistry. We study its interfaces with multiple facets of the metals Ag, Cu, Pt, and Rh using density functional theory calculations; the structures reported shed new light on experimental observations and underscore the importance of solvent−solvent interactions at high coverage. We investigate the relationship of potential of zero charge (PZC) to metal work function, reporting results in agreement with experimental measurements. We develop a model to explain the effects of solvent chemisorption and orientation on the PZC to within a mean absolute deviation of 0.08−0.12 V for all facets studied. Our electrostatic field dependent phase diagram agrees with spectroscopic observations and sheds new light on electrostatic field effects. This work provides new insight into experimental observations on acetonitrile metal interfaces and provides guidance for future studies of acetonitrile and other nonaqueous solvent interfaces with transition metals.

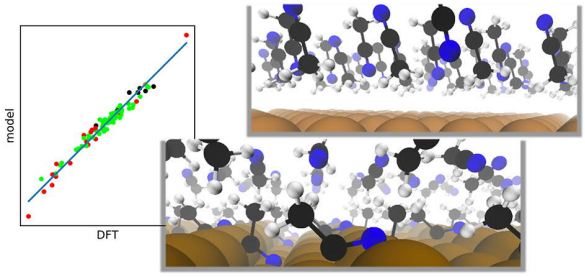

Metal−solvent interfaces are important in a variety of technological applications. The composition of the solvent can critically influence the performance of electrochemical processes.[1,2] Among nonaqueous solvents, acetonitrile is commonly used.[1−29,29−32] The use of acetonitrile to enhance or control the performance of complex electrochemical reactions such as oxygen reduction,[1,4−9,30] carbon dioxide reduction,[2,14−23,23−26,31] and various oxidation reactions[10−13,28,32] is of active research interest. Understanding the effects of nonaqueous solvents, including acetonitrile, on surface electrochemistry is thus a crucial step toward engineering catalytic and electrochemical systems for optimal performance.

Electrochemical and spectroscopic methods have been the primary experimental tools for fundamental experimental investigations of metal−solvent interactions. Electrochemical evidence indicates that acetonitrile chemisorption takes place on transition metals such as Pt, Pd, and Fe, in contrast to a weaker interaction without significant chemisorption on Au, Ag, Bi, Ga, Hg, and other sp-metals.[5,33−48] The relationship of potential of zero charge (PZC) in various solvents to vacuum work function has been of fundamental interest in the study of metal−solvent interactions, as well as of practical importance in electrochemical applications.[49−53] In acetonitrile, it was observed that among Ag and the sp-metals, the PZC depends linearly on the work function, whereas other transition metals such as Pt and Pd deviate substantially from this linear relationship; the deviations are hypothesized to be caused by differences in chemisorption across different groups of metals.[34,38,41,50,54−57] Vibrational and X-ray photoelectron spectroscopy[41,56−61,61−71] corroborate that only weak adsorption without chemical bonding occurs on Au, while at least two chemisorbed species are observed on Pt, Pd, and Ni surfaces: a "bridged" di-sigma-bonded species and a "linear" adsorption, oriented roughly normal to the surface plane and coordinated through the lone electron pair of the N atom, with distinct CN stretching frequency ranges. Potential and charge dependent spectra have also been observed,[5,41,46,63,69,72,73] providing evidence of potential and field dependence of adsorption configurations. But it is difficult to conclusively and unambiguously translate all of the available experimental evidence into a clear understanding of the atomic structure of the interface; this provides motivation for theoretical study of these interfaces.

Density functional theory (DFT) has been widely applied to study the structure of metal surfaces due to a balance of computational expense and accuracy.[74] DFT has been applied to study acetonitrile interactions with Pt, Si, and TiO_2.[5,9,29,75−81] With few exceptions such as a binding energy coverage dependence study on Pt[5] and DFT-based molecular dynamics studies on TiO_2,[79] previous works generally studied low coverages and isolated acetonitrile molecules, rather than full coverage solvent layers corresponding to the metal−liquid interface. At low coverages, distances between adsorbed acetonitrile molecules are large and the corresponding

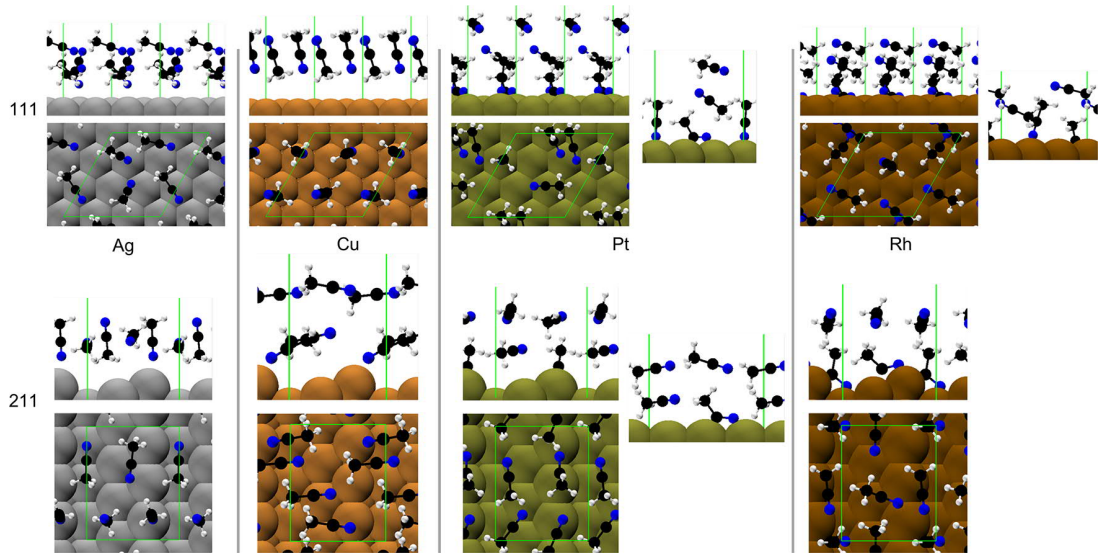

Figure 1. Global minima structures found for acetonitrile−metal interfaces. The simulation supercell periodic boundaries are displayed as green lines. Additional perspectives are shown for the Pt and Rh cases to more clearly display the adsorption configurations.

adsorbate−adsorbate interactions are thus weak; thus the relative stabilities of the possible adsorbate configurations depend predominantly on the adsorbate−surface interactions. At higher coverage, the distance between adsorbates decreases and the interactions between adsorbates becomes significant in determining the overall energy and therefore the structure, in competition with purely adsorbate−surface interactions. There has not been a systematic study of the interfaces of acetonitrile with multiple transition metals and facets at full coverage from first-principles, despite their current relevance in electrochemical technologies.

This study contributes a comprehensive, systematic theoretical study of the fully solvated acetonitrile metal interface on a variety of transition metals (Ag, Cu, Pt, Rh) and facets ((111) and (211), representative close-packed and stepped facets). We apply a global optimization algorithm[82,83] to thoroughly sample physically relevant structures for each interface. We describe the work function−PZC relationship across metals and facets. We explain the collective effects of chemisorption and solvent orientation on the solvated work function and PZC by fitting the numerous local minima to a simple model, with a mean absolute deviation (MAD) of 0.08−0.12 eV for all metals and facets considered. We also investigate the preferred adsorption structure as a function of electrostatic field, indicating the sensitivity of chemisorbed structures on electrostatic fields that may be induced by ions or other adsorbates. And we compare our results to relevant experimental observations, finding consistent results and providing insight into the complex structures of the acetonitrile transition metal interfaces and their properties.

We begin by describing the globally optimized acetonitrile transition metal interfaces. We generated 100 local minima for each surface using minima hopping.[82,83] The structures of the global minima are shown in Figure 1. A summary of chemisorbed configurations and coverages is provided in Table 1. No chemisorption is observed on either Ag facet or on Cu(111), and in general chemisorption coverage increases in the order Ag → Cu → Pt → Rh for both facets. Note that although visually the step edge of Ag(211) appears to adsorb a linear acetonitrile, the closest N−Ag distance on Ag(211) is 2.7 Å, much longer than the N-metal distances on on Cu(211), Pt and Rh, of ≈2.0−2.1 Å. This significantly greater N−metal distance on Ag indicates relatively smaller orbital overlap and thus less chemical bonding character; the density of states analysis investigating this is provided in the Supporting Information. Therefore, we do not categorize this as a chemisorption in Table 1. Two easily distinguishable types of chemisorbed acetonitrile species are observed; one is linear and binds through N, and the other is bent and binds through both C and N, consistent with previous findings. The diversity of configurations and orientations observed among adsorbed and non-adsorbed acetonitrile molecules suggests that interactions among chemisorbed, and non-chemisorbed, acetonitrile species at high coverages become important in determining the overall structure. On Cu(111), for example, the non-chemisorbed acetonitrile molecules assemble into an alternating antiparallel pattern to maximize dipole−dipole interactions between solvent molecules, and Pt and Rh display mixed coverages of strongly chemisorbed linear and bent configurations due to steric and dipole−dipole interactions. We calculated the energies of dipole−dipole interactions between an isolated pair of acetonitrile molecules, as well as the dipole induced dipole interaction of an acetonitrile molecule physisorbed parallel to a metal surface and found that both of these interactions were approximately 0.2 eV in strength. This provides further insight into the driving forces

Table 1. Summary of Acetonitrile Chemisorption on Transition Metal Facets

facet	total ads	linear ads	bent ads	surface atom coord	step edge coord
Ag(111)	0	0	0	0/9 (0%)	
Cu(111)	0	0	0	0/9 (0%)	
Pt(111)	2	1	1	3/9 (33%)	
Rh(111)	2	1	1	4/9 (44%)	
Ag(211)	0	0	0	0/9 (0%)	0/3 (0%)
Cu(211)	1	1	0	1/9 (11%)	1/3 (33%)
Pt(211)	1	0	1	2/9 (22%)	2/3 (67%)
Rh(211)	2	0	2	7/9 (78%)	3/3 (100%)

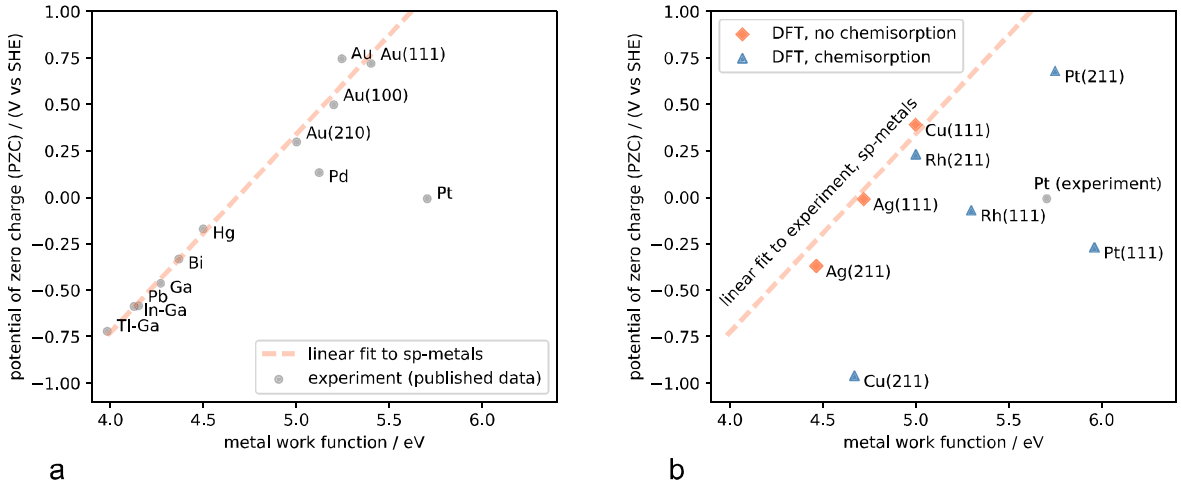

Figure 2. Relationship between metal work function and PZC (a) from previously published experimental results[34,41,55] and (b) from our DFT results, with comparison to the linear fit to experimental results for Au and the sp-metals.

for the competition between the adsorbate−adsorbate and adsorbate−surface interactions at high coverage.

Next we discuss the work function−PZC relationship. The PZC on an absolute scale is approximated by the solvated work function when no excess charge is present.[51−53,84] The PZC on a standard hydrogen electrode (SHE) scale is thus obtained by subtracting the absolute potential of the SHE, a quantity that remains a matter of open research.[84−88] Here we use the value 4.3 V, which has been recently indicated.[86−88] This choice does not affect the relative trends among our DFT results but uniformly shifts the DFT results on an SHE scale. Previous theoretical[89] and experimental work[51,52] has shown that the effect of solvent on the metal work function is largely accounted for by the first layer of solvent in direct contact with the metal. The bulk phase of a conventional solvent is isotropic; therefore, it has no net orientation and thus has no contribution to the electrode potential other than via its interfaces. Our results are summarized in Figure 2.

Previously reported experimental results[34,41,55] are displayed in Figure 2a; our DFT results are displayed in Figure 2b. Here we discuss three main points in comparison with experimental results:

1. the linear trend of non-chemisorbing surfaces,
2. the deviations of chemisorbing surfaces from this line, and
3. the trend among facets of a non-chemisorbing metal.

A linear relationship is apparent among the experimental results for sp-metals and Au, whereas transition metals such as Pd and Pt significantly deviate from this relationship; this observation has been previously discussed.[34,41,55,90] We demonstrate in Figure 2b that our DFT results for non-chemisorbing facets also fall on this same line. Thus, the DFT results for non-chemisorbing surfaces are consistent with the sp-metal trend from experiments. Our DFT results for chemisorbing surfaces deviate from this non-chemisorbing line in the direction of lower PZC. This is consistent with available experimental results, as indicated by the negative deviations of Pd and Pt from the sp-metal trend line. This decrease in PZC has been previously hypothesized to result from electron donation from chemisorbed solvent to the metal surface and possible solvent orientation effects.[34,38] Finally, we compare the facet dependence of a non-chemisorbing metal. The only metal we studied on which acetonitrile does not chemisorb on either facet studied is Ag. We observe a trend of increasing PZC and work function for Ag(211) → Ag(111). This trend is caused by the trend in work functions of these facets and the lack of chemisorption among these facets; changes in the work function thus propagate directly to changes in the PZC. This trend is consistent with the experimentally observed facet trend on Au of increasing work function and PZC on gold in the order of increasingly coordinated facets Au(210) → Au(100) → Au(111).[41,91] Thus, our results are consistent with the experimental findings for the linear trend of non-chemisorbing surfaces, the deviations from this trend caused by chemisorption, and the trend among facets of a given non-chemisorbing metal. But there remains an unexplained and apparently nonlinear relationship between work function and PZC for the strongly chemisorbing facets.

To explain the origins of that more complicated chemisorbing metal relationship in more detail, we build a model to describe variations in the PZC caused by solvent chemisorption and orientation. The form of the model is displayed in eq 1.

$$\Phi_{\text{solvated}} = b + \sum_i N_i(m_i\theta_i + b_i) + c_j\mathbf{1}\left[\sum_i N_i = j\right]$$
$$i \in \{\text{configurations}\} \quad (1)$$

This equation incorporates two solvent contributions (chemisorption and orientation) from each configuration i: not-adsorbed, linear (adsorbed), and bent (adsorbed). N_i is the number of molecules in configuration i per supercell. The quantity θ is the cosine of the angle of the C−N bond vector with the surface normal, representing the surface-normal-component of the C−N orientation. The term θ_i is the average of that quantity, averaged over all species of configuration i which are present. The permanent intrinsic dipole moment of acetonitrile is aligned along the C−N bond, with N the negative end and C the positive end. It is well-known that near metal surfaces, dipoles aligned normal to the surface are reinforced by the image charges induced in the metal whereas dipoles aligned parallel to the surface are canceled out by the image charges induced in the metal. Furthermore, only the

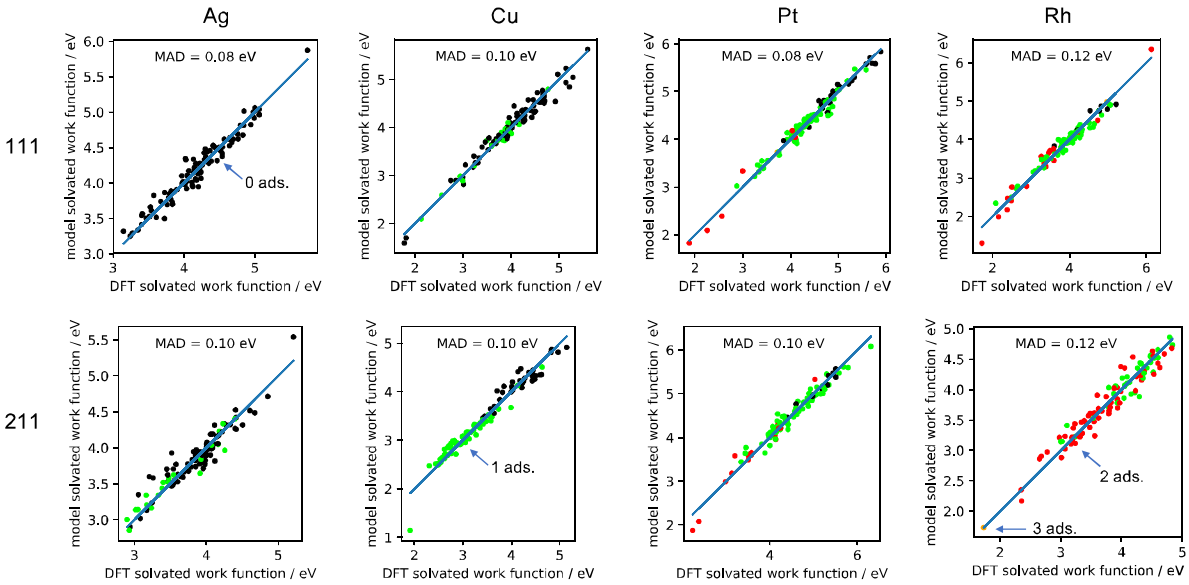

Figure 3. Parity plots (model predicted vs DFT calculated) for model of solvated work function. Marker colors organize data by total number of adsorbed species, visually indicating that the quality of fit is relatively independent of the number of adsorbed species (per supercell).

surface-normal component of the surface dipole moment density contributes to the solvated work function, and thus the PZC. Thus, the quantity $N_i\theta_i$ represents the sum of the components of the permanent dipole moments of the species of configuration i that are normal to the surface and thus can contribute to the total surface dipole moment density. Those considerations provide the physical justification for the form of the orientation term, which aims to capture the effect of the solvent dipole orientation normal to the surface on the PZC. The terms $m_iN_i\theta_i$ thus model the effect of the combined orientations of molecules of a given type, where m_i depends primarily on the intrinsic dipole moment of the solvent since it provides the relationship between the solvent orientation and its effect on the work function. The terms N_ib_i model any additional effect of chemisorption beyond its effect on the orientation of solvent dipoles. Chemisorption of a solvent molecule in a particular configuration could induce polarization of either the adsorbate or the metal surface, or result in a net charge transfer between the adsorbate and surface. Either of these effects would result in a change in charge distribution and thus an effect on the solvated work function, or PZC. Therefore, the coefficient b_i models the effect of charge redistribution per chemisorbed species coverage; the term N_ib_i thus represents the total effect of chemisorption assuming the effect is linear in coverage, in addition to whatever orientation effect chemisorption induces. Finally, the interaction term $\mathbf{1}[\sum_i N_i = j]$ accounts for the effect of adsorbate−adsorbate interactions, or nonlinearity with coverage; the function $\mathbf{1}[\sum_i N_i = j]$ is an indicator function equal to 1 whenever $\sum_i N_i = j$ and is only active when there are more than 1 adsorbed species per supercell. This term is required when the effect of chemisorption does not remain constant as the coverage of chemisorbed species increases. In other words, the interaction term accounts for the possible effects of interactions between chemisorbed molecules as the coverage increases. A more detailed explanation of this model is provided in the Supporting Information for the interested reader. We fit the model parameters m_i, c_j, b_i, b for eq 1 for each metal facet using least-squares. The resulting model explains the effect of adsorption and orientation on the PZC with a MAD of between 0.08 and 0.12 eV, as summarized in parity plots in Figure 3. The configurations studied have PZCs that span a range of at least 3−4 eV, so the MAD of ≈0.1 eV indicates that the model accurately describes much of the variation in this data. Parameter values are tabulated in the Supporting Information. We summarize the key physical insights that arise from the fitted model here:

1. The effect on the PZC of orientation of non-adsorbed species is approximately the same for all metals.
2. The effects on the PZC of linear adsorption are similar for all metals, and the orientation dependence is slightly stronger than that of the non-chemisorbed species, indicating a stronger effective dipole moment.
3. Both linear and bent chemisorption generally decrease the PZC at low coverage, but this effect is nonlinear in coverage.
4. The overall intercept terms b of all surfaces correlate closely with their vacuum work functions, underscoring that solvent orientation and chemisorption effects cause the deviations from the linear relationship for non-chemisorbing surfaces.

Further elaboration on these conclusions based on the fitted model parameters is provided in the Supporting Information. Our results show that the PZC depends sensitively on chemisorption and orientation of species at the surface, which has been hypothesized experimentally,[34] underscoring the importance of thoroughly sampling many possible configurations to globally optimize the structure.

The above results pertain to the structure at the PZC due to the lack of excess surface charge, but at electrode potentials significantly far from the PZC, significant external electric fields can exist at the metal−solvent interface, and there is experimental evidence that this affects the interface structure.[5,46,63,67,68,72,73] We thus study the effect of electrostatic fields on the chemisorbed species on each facet. Field dependence of chemisorbed acetonitrile structure on Pt(111)

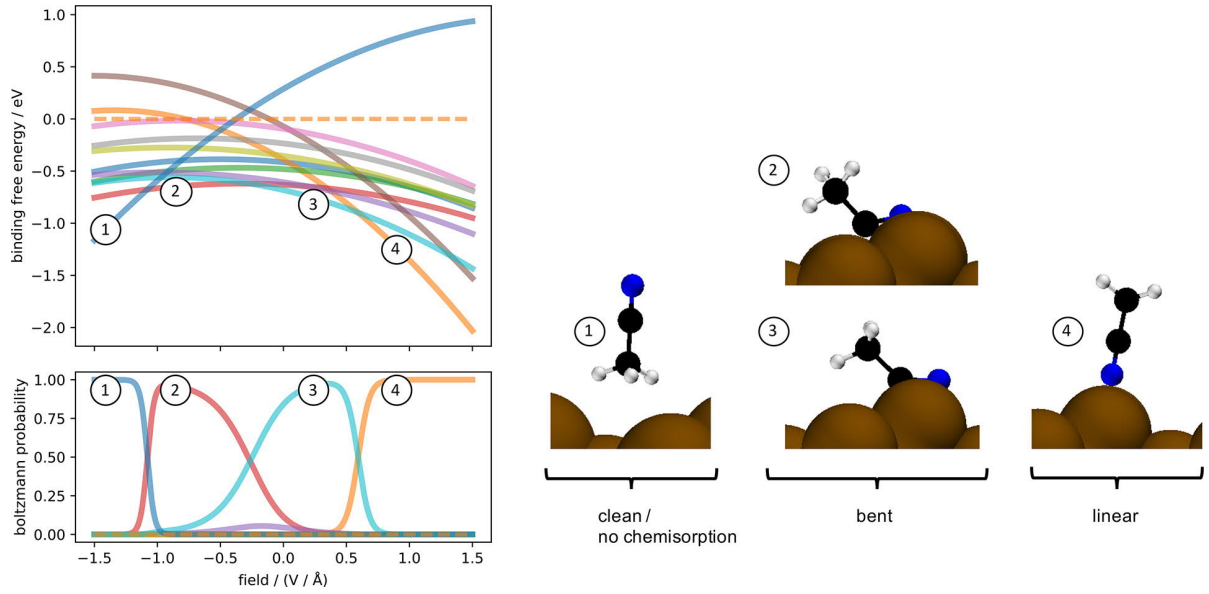

Figure 4. Field dependent binding energies and resulting probabilities on Rh(211) for all configurations tried. The dashed line is the reference state of gas-phase acetonitrile and bare surface. The configurations that have appreciable probabilities are labeled and shown. The dashed line represents acetonitrile in the vapor phase, at equilibrium with liquid acetonitrile at 300 K.

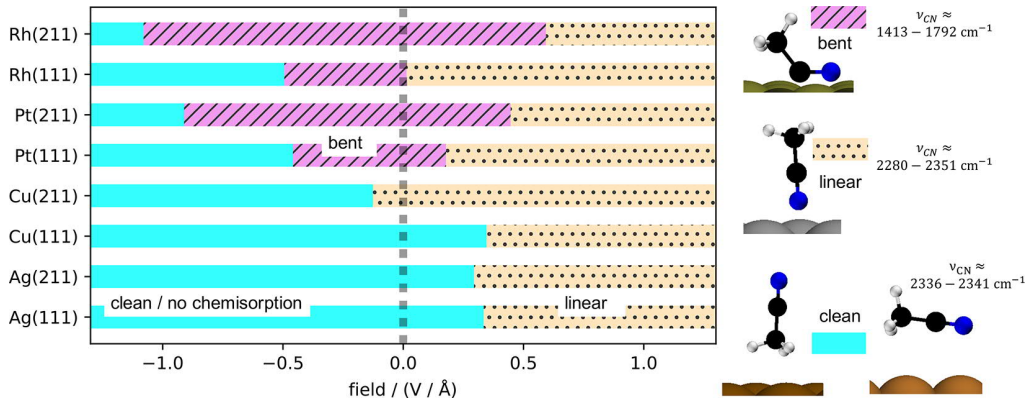

Figure 5. Electrostatic field dependence of adsorbed conformation of acetonitrile on (111) and (211) fcc transition metal facets. The vertical dashed line indicates zero field/PZC.

has already been investigated using DFT;[75] here we extend these results to other metals and facets, including the stepped (211) facets. The binding energies are calculated as a function of electrostatic field as shown in Figure 4; this was done for all surfaces. The resulting phase diagram as a function of electrostatic field is shown in Figure 5.

The phase diagram in Figure 5 is consistent with the observed global minima shown in Figure 1; the facets that do not display chemisorption are reported to be clean at the zero field state, corresponding to the PZC. From Figure 1, on Cu(211) the global minima configuration shows a linear adsorbate, Rh(211) has two bent adsorbates, and Pt(211) has one bent adsorbate, all consistent with the dominant adsorbate at 0 field from Figure 5. Global minima of Rh(111) and Pt(111) in Figure 1 show a mix of linear and bent adsorbates, reflecting that the linear and bent states both appear quite close to the PZC on Figure 5. Positive electrostatic fields (which are present at positive electrode potential relative to PZC) promote the linear adsorption configuration, which has a greater positive surface dipole moment than that of the bent state (we use the convention that "positive dipole moment" means that the positive end is directed away from the surface). We also note that the positive surface dipole moment of both adsorbed species is consistent with the experimental observation that chemisorption of acetonitrile lowers the work function[34,38] as mentioned earlier.

We now compare the field-dependent phase diagram with selected experimental results. The non-chemisorbing facets Ag(111), Ag(211), and Cu(111), which appear to have very similar behavior in Figure 5, display no chemisorption at negative fields or fields less than ≈0.3 V/Å. At fields more positive than ≈0.3 V/Å, a linear N-down chemisorbed state becomes energetically favorable. Experiments demonstrate that on Au, acetonitrile weakly physisorbs with no evidence of chemisorption on the neutral and negatively charged electrode (corresponding to negative field strengths in Figure 5);[41,56,57,67,68] N-down linear chemisorption occurs only at positive electrode charge above approximately 8 μC cm^{-2} (corresponding to positive field in Figure 5).[41,69] In fact, Figure 5 demonstrates that Cu(211) shows the same

qualitative behavior: no chemisorption at sufficiently negative electrostatic field, and linear, N-down chemisorption at sufficiently positive electrostatic field. Thus, our results for Ag and Cu are in agreement with available experimental data for group 11 (coinage) metals.

Next we consider the more strongly binding metals Pt and Rh, which demonstrate behavior qualitatively different from that of Ag and Cu. Near the PZC and at low field strengths, there is an electrostatic field range within which the bent configuration dominates. At fields positive of this bent regime, the linear configuration dominates, and at sufficiently negative fields, acetonitrile desorbs, flipping N-up to align the permanent dipole moment with the field. The bent configuration is stable over a broader range of fields on the (211) facet than on the (111) facet for both Pt and Rh. Thus, step sites stabilize the bent configuration relative to both the desorbed, N-up configuration and the linear chemisorbed configuration. Our results are consistent with previous experimental and theoretical evidence that on Pt acetonitrile adsorbs in the linear N-down form at potentials positive of the PZC and in the bent form at potentials near and slightly negative of the PZC, and it desorbs to flip N-up at strongly negative fields.[72,75] Our results show that this behavior extends to both facets of Pt and Rh, including on steps. More generally, the existence of both linear and bent chemisorbed species has been experimentally demonstrated on Pt, Pd, and Ni surfaces[58−61,61−64] and for methyl isocyanide on Rh;[92] our results show that both forms are stable on the surface at conditions relatively close to the PZC and thus are consistent with those observations. We also note that the vibrational frequencies from DFT are consistent with experiment: the CN stretching mode of the bent configuration is strongly red-shifted.[65,66] Vibrational modes are provided in the Supporting Information.

Finally, we investigate the physical origins of the effect of chemisorption on the PZC, which we empirically described by the model presented in eq 1 and Figure 3. We posit two hypotheses for the origins of the effect of chemisorption of solvent on the PZC:

1. The chemisorbed configurations of the solvent have intrinsic dipole moments arising from the charge distribution within the adsorbate itself; the contribution of these adsorbate dipole moments to the surface dipole moment density has an effect on the PZC, and

2. The redistribution of charge density due to chemisorption: both the metal surface and the adsorbate could be polarized by their interaction, and charge can be transferred between the adsorbate and the surface. This too would result in a surface dipole moment density with an effect on the PZC.

To investigate the relative importance of these two possible physical origins, we perform single point calculations on the chemisorbed solvent configurations studied in the phase diagram for each surface. We compare the effective dipole moments of the adsorbed solvent configurations on their respective metal surfaces to those configurations in the absence of the surface (in a vacuum) with the work functions. We also approximate any charge transfer between the adsorbate and the surface using Bader charge analysis.[93−96] The results for the Bader charge as well as the gas-phase and adsorbed surface dipole moments (in the z-direction) are provided in Table 2.

Table 2. Charge Transfer to Adsorbate, Adsorbate Surface Dipole Moment, and Change in Surface Dipole Moment Induced by Chemisorption Relative to the Same Configuration in the Gas Phase, for Linear and Bent Adsorbates on All Facets Studied

facet	config.	charge transfer to adsorbate/e	adsorbate surface dipole moment/e Å	change in dipole moment from adsorption/e Å
Ag(111)	linear	−0.01	0.84	0.09
Ag(211)	linear	−0.01	0.74	0.10
Cu(111)	linear	−0.03	0.72	0.10
Cu(211)	linear	−0.04	0.51	0.14
Pt(111)	bent	−0.20	0.23	−0.08
Pt(111)	linear	0.03	0.87	0.19
Pt(211)	bent	−0.23	0.21	−0.09
Pt(211)	linear	−0.01	0.89	0.18
Rh(111)	bent	−0.48	0.18	−0.18
Rh(111)	linear	−0.07	0.77	0.04
Rh(211)	bent (i)	−0.50	0.06	−0.17
Rh(211)	bent (ii)	−0.35	0.27	−0.16
Rh(211)	linear	−0.09	0.70	−0.01

These results indicate that most of the chemisorbed surface dipole moment, and thus the effect on the PZC, are explained purely by the chemisorbed configuration of the adsorbate; the dipole moments without the surface present are in general quite similar to those of the adsorbed species. For both linear and bent configurations, this surface dipole moment is positive, consistent with a decrease in the PZC concomitant with chemisorption. Negative charge is transferred to the bent adsorbate from the metal; there is nearly zero net charge transfer between the linear adsorbate and the metal surface. Adsorption to the metal surface has a small polarization effect on the adsorbed species; adsorption increases the positive dipole moment in the linear configuration and diminishes the positive dipole moment in the bent configuration, consistent with the negative charge that is transferred to the bent configuration. But our results indicate that in general this effect is relatively smaller than that of the intrinsic dipole of the adsorbed species due to its orientation.

More detailed descriptions of the field-dependent binding energies are provided in the Supporting Information; these are important for determining competing adsorption equilibria among other possible adsorbed species. Acetonitrile chemisorption does not fully cover even surfaces on which it is strongly bound at low coverage, as reported here in Figure 1 and Table 1; this is consistent with previously reported repulsive adsorbate−adsorbate interactions at higher coverages.[5] We also did not consider possible reactive/dissociative chemisorption[45−47] or any electrochemical steps involving other species such as hydroxide or hydrogen ions,[9] as we aimed to model the pure acetonitrile metal interface, investigating only molecular adsorption steps. Finally, it should be noted that the current work focused on examining structure using static local minima rather than using molecular dynamics simulations,[79] which could provide more detailed structural data regarding the effect of thermal fluctuations, which may be important especially for the non-chemisorbed species. The fundamental understanding of acetonitrile transition metal interfaces contributed by this work should provide guidance for future studies incorporating the complexities just mentioned.

COMPUTATIONAL DETAILS

Quantum ESPRESSO[97,98] was used for DFT calculations with the dispersion-corrected Bayesian error estimation functional (BEEF),[74,99−101] the atomic simulation environment (ASE) was used for minima hopping calculations and thermochemistry analysis,[102] and figures were produced using VMD.[103] Valence electrons were represented by a plane wave basis set, Vanderbilt ultrasoft pseudopotentials were used for core electrons,[104−107] and the Brillouin zone was sampled using a Monkhorst Pack k-point grid.[108] Further details are provied in the Supporting Information.

For the (111) facets, a 3 × 3 (9 surface atoms) supercell was used; for the (211) facets, a 3 atom × 3 atom (3 step edge atoms; 9 surface atoms total) supercell was constructed. We included four acetonitrile molecules per simulation supercell, as this corresponded to at least one full solvent layer on the surfaces studied; more acetonitrile molecules would not fit in contact with the metal surface. We applied the minima hopping algorithm[82,83] as described in previous work[89] to generate 100 local minima each for the (211) and (111) facet of each metal.

AUTHOR INFORMATION

Corresponding Author

Jens K. Nørskov − *Department of Physics, Technical University of Denmark, DK-2800 Kongens Lyngby, Denmark;* orcid.org/0000-0002-4427-7728; Email: jkno@fysik.dtu.dk

Authors

Thomas Ludwig − *SUNCAT Center for Interface Science and Catalysis, SLAC National Accelerator Laboratory, Menlo Park, California 94025, United States; SUNCAT Center for Interface Science and Catalysis, Department of Chemical Engineering, Stanford University, Stanford, California 94305, United States;* orcid.org/0000-0002-2921-0488

Aayush R. Singh − *SUNCAT Center for Interface Science and Catalysis, SLAC National Accelerator Laboratory, Menlo Park, California 94025, United States; SUNCAT Center for Interface Science and Catalysis, Department of Chemical Engineering, Stanford University, Stanford, California 94305, United States;* orcid.org/0000-0003-0442-9691

Notes

The authors declare no competing financial interest.

ACKNOWLEDGMENTS

This research was supported by the U.S. Department of Energy, Office of Science, Office of Basic Energy Sciences, Chemical Sciences, Geosciences, and Biosciences Division, Catalysis Science Program to the SUNCAT Center for Interface Science and Catalysis. T.L. acknowledges support from the United States Department of Energy through the Computational Sciences Graduate Fellowship (DOE CSGF) under grant number DE-FG02-97ER25308. We thank Stanford University and the Stanford Research Computing Center for providing computational resources and support that contributed to these research results.

REFERENCES

(1) Laoire, C. O.; Mukerjee, S.; Abraham, K.; Plichta, E. J.; Hendrickson, M. A. Influence of nonaqueous solvents on the electrochemistry of oxygen in the rechargeable lithium- air battery. *J. Phys. Chem. C* **2010**, *114*, 9178−9186.

(2) König, M.; Vaes, J.; Klemm, E.; Pant, D. Solvents and supporting electrolytes in the electrocatalytic reduction of CO2. *Iscience* **2019**, *19*, 135−160.

(3) Reshetenko, T. V.; St-Pierre, J. Study of the acetonitrile poisoning of platinum cathodes on proton exchange membrane fuel cell spatial performance using a segmented cell system. *J. Power Sources* **2015**, *293*, 929−940.

(4) Smiljanić, M. L.; Srejić, I. L.; Marinović, V. M.; Rakočević, Z. L.; Štrbac, S. B. Inhibiting effect of acetonitrile on oxygen reduction on polycrystalline Pt electrode in sodium chloride solution. *Hem. Ind.* **2012**, *66*, 327−333.

(5) Pašti, I. A.; Marković, A.; Gavrilov, N.; Mentus, S. V. Adsorption of acetonitrile on platinum and its effects on oxygen reduction reaction in acidic aqueous solutions—combined theoretical and experimental study. *Electrocatalysis* **2016**, *7*, 235−248.

(6) Ge, J.; St-Pierre, J.; Zhai, Y. PEMFC cathode catalyst contamination evaluation with a RRDE-Acetonitrile. *Electrochim. Acta* **2014**, *134*, 272−280.

(7) Srejić, I.; Smiljanić, M.; Rakočević, Z. L.; Štrbac, S. Oxygen reduction on polycrystalline Pt and Au electrodes in perchloric acid solution in the presence of acetonitrile. *Int. J. Electrochem. Sci.* **2011**, *6*, 3344−3354.

(8) Li, Q.; Batchelor-McAuley, C.; Lawrence, N. S.; Hartshorne, R. S.; Compton, R. G. Anomalous solubility of oxygen in acetonitrile/water mixture containing tetra-n-butylammonium perchlorate supporting electrolyte; the solubility and diffusion coefficient of oxygen in anhydrous acetonitrile and aqueous mixtures. *J. Electroanal. Chem.* **2013**, *688*, 328−335.

(9) Briega-Martos, V.; Costa-Figueiredo, M.; Orts, J. M.; Rodes, A.; Koper, M. T.; Herrero, E.; Feliu, J. M. Acetonitrile adsorption on Pt single-crystal electrodes and its effect on oxygen reduction reaction in acidic and alkaline aqueous solutions. *J. Phys. Chem. C* **2019**, *123*, 2300−2313.

(10) Briega-Martos, V.; Solla-Gullón, J.; Koper, M. T.; Herrero, E.; Feliu, J. M. Electrocatalytic enhancement of formic acid oxidation reaction by acetonitrile on well-defined platinum surfaces. *Electrochim. Acta* **2019**, *295*, 835−845.

(11) Angerstein-Kozlowska, H.; MacDougall, B.; Conway, B. Origin of activation effects of acetonitrile and mercury in electrocatalytic oxidation of formic acid. *J. Electrochem. Soc.* **1973**, *120*, 756.

(12) Wasmus, S.; Vielstich, W. Influence of acetonitrile, dimethylsulfoxide and lead on the electro-oxidation of small organic molecules: an on-line mass spectroscopy study. *J. Electroanal. Chem.* **1993**, *359*, 175−191.

(13) Ledezma-Yanez, I.; Díaz-Morales, O.; Figueiredo, M. C.; Koper, M. T. Hydrogen oxidation and hydrogen evolution on a platinum electrode in acetonitrile. *ChemElectroChem* **2015**, *2*, 1612−1622.

(14) Mendieta-Reyes, N. E.; Díaz-García, A. K.; Gómez, R. Simultaneous electrocatalytic CO2 reduction and enhanced electrochromic effect at WO3 nanostructured electrodes in acetonitrile. *ACS Catal.* **2018**, *8*, 1903−1912.

(15) Figueiredo, M. C.; Ledezma-Yanez, I.; Koper, M. T. In situ spectroscopic study of CO2 electroreduction at copper electrodes in acetonitrile. *ACS Catal.* **2016**, *6*, 2382−2392.
(16) Zhu, Q.; Ma, J.; Kang, X.; Sun, X.; Liu, H.; Hu, J.; Liu, Z.; Han, B. Efficient reduction of CO2 into formic acid on a lead or tin electrode using an ionic liquid catholyte mixture. *Angew. Chem.* **2016**, *128*, 9158−9162.
(17) Zhu, Q.; Ma, J.; Kang, X.; Sun, X.; Hu, J.; Yang, G.; Han, B. Electrochemical reduction of CO 2 to CO using graphene oxide/carbon nanotube electrode in ionic liquid/acetonitrile system. *Sci. China: Chem.* **2016**, *59*, 551−556.
(18) Rudnev, A. V.; Zhumaev, U. E.; Kuzume, A.; Vesztergom, S.; Furrer, J.; Broekmann, P.; Wandlowski, T. The promoting effect of water on the electroreduction of CO2 in acetonitrile. *Electrochim. Acta* **2016**, *189*, 38−44.
(19) Díaz-Duque, Á.; Sandoval-Rojas, A. P.; Molina-Osorio, A. F.; Feliu, J. M.; Suárez-Herrera, M. F. Electrochemical reduction of CO2 in water-acetonitrile mixtures on nanostructured Cu electrode. *Electrochem. Commun.* **2015**, *61*, 74−77.
(20) Matsubara, Y.; Grills, D. C.; Kuwahara, Y. *ACS Catal.* **2015**, *5*, 6440−6452.
(21) Berto, T. C.; Zhang, L.; Hamers, R. J.; Berry, J. F. Electrolyte dependence of CO2 electroreduction: tetraalkylammonium ions are not electrocatalysts. *ACS Catal.* **2015**, *5*, 703−707.
(22) Sun, L.; Ramesha, G. K.; Kamat, P. V.; Brennecke, J. F. Switching the reaction course of electrochemical CO2 reduction with ionic liquids. *Langmuir* **2014**, *30*, 6302−6308.
(23) Oh, Y.; Vrubel, H.; Guidoux, S.; Hu, X. Electrochemical reduction of CO 2 in organic solvents catalyzed by MoO 2. *Chem. Commun.* **2014**, *50*, 3878−3881.
(24) Lv, W. X.; Zhang, R.; Gao, P. R.; Gong, C. X.; Lei, L. X. Electrochemical reduction of carbon dioxide on stainless steel electrode in acetonitrile. *Adv. Mater. Res.* **2013**, *807-809*, 1322−1325.
(25) Tomita, Y.; Teruya, S.; Koga, O.; Hori, Y. Electrochemical reduction of carbon dioxide at a platinum electrode in acetonitrile-water mixtures. *J. Electrochem. Soc.* **2000**, *147*, 4164.
(26) Aylmer-Kelly, A.; Bewick, A.; Cantrill, P.; Tuxford, A. Studies of electrochemically generated reaction intermediates using modulated specular reflectance spectroscopy. *Faraday Discuss. Chem. Soc.* **1973**, *56*, 96−107.
(27) Jackson, M. N.; Surendranath, Y. Donor-dependent kinetics of interfacial proton-coupled electron transfer. *J. Am. Chem. Soc.* **2016**, *138*, 3228−3234.
(28) Schiffer, Z. J.; Lazouski, N.; Corbin, N.; Manthiram, K. Nature of the first electron transfer in electrochemical ammonia activation in a nonaqueous medium. *J. Phys. Chem. C* **2019**, *123*, 9713−9720.
(29) Yamada, Y.; Furukawa, K.; Sodeyama, K.; Kikuchi, K.; Yaegashi, M.; Tateyama, Y.; Yamada, A. Unusual stability of acetonitrile-based superconcentrated electrolytes for fast-charging lithium-ion batteries. *J. Am. Chem. Soc.* **2014**, *136*, 5039−5046.
(30) Peng, Z.; Freunberger, S. A.; Hardwick, L. J.; Chen, Y.; Giordani, V.; Bardé, F.; Novák, P.; Graham, D.; Tarascon, J.-M.; Bruce, P. G. Oxygen reactions in a non-aqueous Li+ electrolyte. *Angew. Chem., Int. Ed.* **2011**, *50*, 6351−6355.
(31) Oh, S.; Gallagher, J. R.; Miller, J. T.; Surendranath, Y. Graphite-conjugated rhenium catalysts for carbon dioxide reduction. *J. Am. Chem. Soc.* **2016**, *138*, 1820−1823.
(32) Jin, K.; Maalouf, J. H.; Lazouski, N.; Corbin, N.; Yang, D.; Manthiram, K. Epoxidation of cyclooctene using water as the oxygen atom source at manganese oxide electrocatalysts. *J. Am. Chem. Soc.* **2019**, *141*, 6413−6418.
(33) Petrii, O.; Khomchenko, I. Electrochemical Properties of Platinum and Palladium Electrodes in Acetonitrile Solutions. *J. Electroanal. Chem. Interfacial Electrochem.* **1980**, *106*, 277−286.
(34) Bagotskaya, I.; Kazarinov, V. Solvent effects in the electric double-layer structure for gallium and gallium-like metals. *J. Electroanal. Chem.* **1992**, *329*, 225−236.
(35) Rudnev, A.; Molodkina, E.; Danilov, A.; Polukarov, Y. M.; Feliu, J. Kinetics of copper UPD on stepped platinum single crystals in the presence of acetonitrile. *Electrochem. Commun.* **2008**, *10*, 502−505.
(36) Rudnev, A.; Molodkina, E.; Danilov, A.; Polukarov, Y. M.; Berna, A.; Feliu, J. Adsorption behavior of acetonitrile on platinum and gold electrodes of various structures in solution of 0.5 M H2SO4. *Electrochim. Acta* **2009**, *54*, 3692−3699.
(37) Song, D.; Soriaga, M. P.; Hubbard, A. T. Effect of non-aqueous solvents on the chemisorption and orientation of aromatic compounds at smooth polycrystalline platinum electrodes: naphthohydroquinone and tetrahydroxybiphenyl in water+ acetonitrile solutions. *J. Electroanal. Chem. Interfacial Electrochem.* **1986**, *201*, 153−162.
(38) Safonov, V.; Komissarov, L. Y.; Petrii, O. Electrical double layer on renewed iron electrodes in solutions based on a number of organic solvents. *Electrochim. Acta* **1997**, *42*, 675−687.
(39) Safonov, V.; Choba, M.; Petrii, O. The difference between interfaces formed by mechanically renewed gold and silver electrodes with acetonitrile and aqueous solutions. *J. Electroanal. Chem.* **2018**, *808*, 278−285.
(40) Doubova, L.; Trasatti, S.; Valcher, S. Adsorption of acetonitrile on polycrystalline Ag electrodes: comparison with Hg electrodes. *J. Electroanal. Chem.* **1993**, *349*, 187−195.
(41) Panzram, E.; Baumgärtel, H.; Roelfs, B.; Schröter, C.; Solomun, T. A capacitance and infrared study of the electrical double layer structure at single crystal gold electrodes in acetonitrile. *Berichte der Bunsengesellschaft für physikalische Chemie* **1995**, *99*, 827−837.
(42) De Battisti, A.; Trasatti, S. Adsorption of acetonitrile at the mercury/aqueous solution interface. Comparison of constant-potential and constant-charge analysis. *J. Electroanal. Chem. Interfacial Electrochem.* **1973**, *48*, 213−238.
(43) Emets, V.; Damaskin, B. The electrical double layer at the Bi−Ga liquid alloy in the acetonitrile electrolyte solutions. *Russ. J. Electrochem.* **2004**, *40*, 1066−1073.
(44) Emets, V.; Mel'nikov, A. Electric double layer on a renewable liquid (Cd−Ga) electrode in acetonitrile solutions. *Russ. J. Electrochem.* **2018**, *54*, 1012−1021.
(45) Morin, S.; Conway, B. Surface structure dependence of reactive chemisorption of acetonitrile on single-crystal Pt surfaces. *J. Electroanal. Chem.* **1994**, *376*, 135−150.
(46) Morin, S.; Conway, B.; Edens, G.; Weaver, M. The reactive chemisorption of acetonitrile on Pt (111) and Pt (100) electrodes as examined by in situ infrared spectroscopy. *J. Electroanal. Chem.* **1997**, *421*, 213−220.
(47) Angerstein-Kozlowska, H.; MacDougall, B.; Conway, B. Electrochemisorption and reactivity of nitriles at platinum electrodes and the anodic H desorption effect. *J. Electroanal. Chem. Interfacial Electrochem.* **1972**, *39*, 287−313.
(48) Conway, B.; MacDougall, B.; Kozlowska, H. Anodic displacement of adsorbed H in electrochemisorption of organic molecules at platinum. *J. Chem. Soc., Faraday Trans. 1* **1972**, *68*, 1566−1582.
(49) Bockris, J. O.; Argade, S. Work function of metals and the potential at which they have zero charge in contact with solutions. *J. Chem. Phys.* **1968**, *49*, 5133−5134.
(50) Trasatti, S. Work function, electronegativity, and electrochemical behaviour of metals: II. Potentials of zero charge and "electrochemical" work functions. *J. Electroanal. Chem. Interfacial Electrochem.* **1971**, *33*, 351−378.
(51) Kaur, J.; Kant, R. Theory of work function and potential of zero charge for metal nanostructured and rough electrodes. *J. Phys. Chem. C* **2017**, *121*, 13059−13069.
(52) Heras, J.; Viscido, L. Work function changes upon water contamination of metal surfaces. *Appl. Surf. Sci.* **1980**, *4*, 238−241.
(53) Trasatti, S. Structure of the metal/electrolyte solution interface: new data for theory. *Electrochim. Acta* **1991**, *36*, 1659−1667.
(54) Trasatti, S. *Trends in Interfacial Electrochemistry*; Springer, 1986; pp 25−48.
(55) Trasatti, S. Effect of the nature of the metal on the dielectric properties of polar liquids at the interface with electrodes. A

phenomenological approach. *J. Electroanal. Chem. Interfacial Electrochem.* **1981**, *123*, 121−139.
(56) Solomun, T.; Christmann, K.; Baumgärtel, H. Interaction of acetonitrile and benzonitrile with the gold (100) surface. *J. Phys. Chem.* **1989**, *93*, 7199−7208.
(57) Solomun, T.; Baumgärtel, H.; Christmann, K. The interaction of nitriles with a potassium-promoted gold (100) surface. *J. Phys. Chem.* **1991**, *95*, 10041−10049.
(58) Friend, C.-M.; Muetterties, E.; Gland, J. Vibrational studies of acetonitrile and methyl isocyanide adsorbed on nickel (111) and nickel (111)-carbon surfaces. *J. Phys. Chem.* **1981**, *85*, 3256−3262.
(59) Sexton, B.; Avery, N. Coordination of acetonitrile (CH3CN) to platinum (111): Evidence for an η2 (C, N) species. *Surf. Sci.* **1983**, *129*, 21−36.
(60) Szilagyi, T. Infrared spectra of methyl cyanide and methyl isocyanide adsorbed on pt/sio2. *Appl. Surf. Sci.* **1988**, *35*, 19−26.
(61) Kosaku, K.; Shigero, I. Adsorption of acetonitrile on evaporated nickel and palladium films studied by X-ray photoelectron spectroscopy. *Surf. Sci.* **1981**, *107*, 405−416.
(62) Kishi, K.; Okino, Y.; Fujimoto, Y. XPS studies of the adsorption of CH3CN and C6H5CN on the Ni (111) surface. *Surf. Sci.* **1986**, *176*, 23−31.
(63) Villegas, I.; Weaver, M. J. Infrared spectroscopy of model electrochemical interfaces in ultrahigh vacuum: ionic versus interfacial solvation by acetone and acetonitrile on Pt (111). *J. Am. Chem. Soc.* **1996**, *118*, 458−466.
(64) Tylinski, M.; Smith, R. S.; Kay, B. D. Structure and desorption kinetics of acetonitrile thin films on Pt (111) and on graphene on Pt (111). *J. Phys. Chem. C* **2020**, *124*, 2521−2530.
(65) Raskó, J.; Kiss, J. Adsorption and surface reactions of acetonitrile on Al2O3-supported noble metal catalysts. *Appl. Catal., A* **2006**, *298*, 115−126.
(66) Aguirre, A.; Collins, S. E. Insight into the mechanism of acetonitrile hydrogenation in liquid phase on Pt/Al2O3 by ATR-FTIR. *Catal. Today* **2019**, *336*, 22−32.
(67) Solomun, T.; Christmann, K.; Neumann, A.; Baumgartel, H. Structural information pertaining to non-aqueous electrified interfaces: 2-D solvation of potassium with nitriles on the Au(100) surface. *J. Electroanal. Chem. Interfacial Electrochem.* **1991**, *309*, 355−363.
(68) Neumann, A.; Rabus, H.; Arvanitis, D.; Solomun, T.; Christmann, K.; Baberschke, K. Alkali-metal-induced bond length contraction of acetonitrile (CH3CN) on Au (100). *Chem. Phys. Lett.* **1993**, *201*, 108−114.
(69) Faguy, P. W.; Fawcett, W. R.; Liu, G.; Motheo, A. J. A study of the adsorption of acetonitrile on a gold electrode from aqueous solutions using in situ vibrational spectroscopy. *J. Electroanal. Chem.* **1992**, *339*, 339−353.
(70) Davidson, T.; Pons, B. S.; Bewick, A.; Schmidt, P. Vibrational Spectroscopy of the Electrode-Electrolyte Interface: Use of Fourier Transform Infrared Spectroscopy. *J. Electroanal. Chem. Interfacial Electrochem.* **1981**, *125*, 237−241.
(71) Pons, S.; Davidson, T.; Bewick, A. Vibrational spectroscopy of the electrode—solution interface: Part III. Use of fourier transform spectroscopy for observing double layer reorganization. *J. Electroanal. Chem. Interfacial Electrochem.* **1982**, *140*, 211−216.
(72) Marinković, N. S.; Hecht, M.; Loring, J. S.; Fawcett, W. R. A SNIFTIRS study of the diffuse double layer at single crystal platinum electrodes in acetonitrile. *Electrochim. Acta* **1996**, *41*, 641−651.
(73) Baldelli, S.; Mailhot, G.; Ross, P.; Shen, Y.-R.; Somorjai, G. A. Potential dependent orientation of acetonitrile on platinum (111) electrode surface studied by sum frequency generation. *J. Phys. Chem. B* **2001**, *105*, 654−662.
(74) Wellendorff, J.; Lundgaard, K. T.; Møgelhøj, A.; Petzold, V.; Landis, D. D.; Nørskov, J. K.; Bligaard, T.; Jacobsen, K. W. Density functionals for surface science: Exchange-correlation model development with Bayesian error estimation. *Phys. Rev. B: Condens. Matter Mater. Phys.* **2012**, *85*, 235149.
(75) Markovits, A.; Minot, C. Theoretical study of the acetonitrile flip-flop with the electric field orientation: adsorption on a Pt (111) electrode surface. *Catal. Lett.* **2003**, *91*, 225−234.
(76) Shayeghi, A.; Krahling, S.; Hortz, P.; Johnston, R.; Heard, C.; Schafer, R. Adsorption of acetonitrile, benzene, and benzonitrile on Pt (111): single crystal adsorption calorimetry and density functional theory. *J. Phys. Chem. C* **2017**, *121*, 21354−21363.
(77) Zou, X.-J.; Ding, K. N.; Zhang, Y. F.; Li, J. Q. A DFT study of acetonitrile adsorption and decomposition on the TiO2 (110) surface. *Int. J. Quantum Chem.* **2011**, *111*, 915−922.
(78) Luber, S. Sum frequency generation of acetonitrile on a rutile (110) surface from density functional theory-based molecular dynamics. *J. Phys. Chem. Lett.* **2016**, *7*, 5183−5187.
(79) Zhang, R.; Dong, J.; Luo, T.; Tang, F.; Peng, X.; Zhou, C.; Yang, X.; Xu, L.; Ren, Z. Adsorption structure and coverage-dependent orientation analysis of sub-monolayer acetonitrile on TiO2 (110). *J. Phys. Chem. C* **2019**, *123*, 17915−17924.
(80) Tao, F.; Wang, Z. H.; Qiao, M. H.; Liu, Q.; Sim, W. S.; Xu, G. Q. Covalent attachment of acetonitrile on Si (100) through Si−C and Si−N linkages. *J. Chem. Phys.* **2001**, *115*, 8563−8569.
(81) Carniato, S.; Rochet, F.; Gallet, J.-J.; Bournel, F.; Dufour, G.; Mathieu, C.; Rangan, S. DFT calculations of XPS/NEXAFS and IR spectra to elucidate the reaction products of acetonitrile with Si (0 0 1)-2× 1. *Surf. Sci.* **2007**, *601*, 5515−5525.
(82) Goedecker, S. Minima hopping: An efficient search method for the global minimum of the potential energy surface of complex molecular systems. *J. Chem. Phys.* **2004**, *120*, 9911−9917.
(83) Peterson, A. A. Global optimization of adsorbate−surface structures while preserving molecular identity. *Top. Catal.* **2014**, *57*, 40−53.
(84) Trasatti, S. The absolute electrode potential: an explanatory note. *Pure Appl. Chem.* **1986**, *58*, 955−966.
(85) Donald, W. A.; Leib, R. D.; O'Brien, J. T.; Bush, M. F.; Williams, E. R. Absolute standard hydrogen electrode potential measured by reduction of aqueous nanodrops in the gas phase. *J. Am. Chem. Soc.* **2008**, *130*, 3371−3381.
(86) Isse, A. A.; Gennaro, A. Absolute potential of the standard hydrogen electrode and the problem of interconversion of potentials in different solvents. *J. Phys. Chem. B* **2010**, *114*, 7894−7899.
(87) Ishikawa, A.; Nakai, H. Quantum chemical approach for condensed-phase thermochemistry (III): Accurate evaluation of proton hydration energy and standard hydrogen electrode potential. *Chem. Phys. Lett.* **2016**, *650*, 159−164.
(88) Hofer, T. S.; Hünenberger, P. H. Absolute proton hydration free energy, surface potential of water, and redox potential of the hydrogen electrode from first principles: QM/MM MD free-energy simulations of sodium and potassium hydration. *J. Chem. Phys.* **2018**, *148*, 222814.
(89) Ludwig, T.; Gauthier, J. A.; Brown, K. S.; Ringe, S.; Nørskov, J. K.; Chan, K. Solvent−adsorbate interactions and adsorbate-specific solvent structure in carbon dioxide reduction on a stepped Cu surface. *J. Phys. Chem. C* **2019**, *123*, 5999−6009.
(90) Rohatgi, A. *WebPlotDigitizer*. **2017**.
(91) Ross, P. N.; D'Agostino, A. T. The effect of surface reconstruction on the capacitance of Au (100) surfaces. *Electrochim. Acta* **1992**, *37*, 615−623.
(92) Semancik, S.; Haller, G.; Yates, J. T., Jr The adsorption and dissociation of methyl isocyanide on Rh (111). *J. Chem. Phys.* **1983**, *78*, 6970−6981.
(93) Tang, W.; Sanville, E.; Henkelman, G. A grid-based Bader analysis algorithm without lattice bias. *J. Phys.: Condens. Matter* **2009**, *21*, 084204.
(94) Sanville, E.; Kenny, S. D.; Smith, R.; Henkelman, G. Improved grid-based algorithm for Bader charge allocation. *J. Comput. Chem.* **2007**, *28*, 899−908.
(95) Henkelman, G.; Arnaldsson, A.; Jónsson, H. A fast and robust algorithm for Bader decomposition of charge density. *Comput. Mater. Sci.* **2006**, *36*, 354−360.

(96) Yu, M.; Trinkle, D. R. Accurate and efficient algorithm for Bader charge integration. *J. Chem. Phys.* **2011**, *134*, 064111.
(97) Giannozzi, P.; et al. QUANTUM ESPRESSO: a modular and open-source software project for quantum simulations of materials. *J. Phys.: Condens. Matter* **2009**, *21*, 395502.
(98) Bengtsson, L. Dipole correction for surface supercell calculations. *Phys. Rev. B: Condens. Matter Mater. Phys.* **1999**, *59*, 12301−12304.
(99) Dion, M.; Rydberg, H.; Schröder, E.; Langreth, D. C.; Lundqvist, B. I. Van der Waals density functional for general geometries. *Phys. Rev. Lett.* **2004**, *92*, 246401.
(100) Thonhauser, T.; Cooper, V. R.; Li, S.; Puzder, A.; Hyldgaard, P.; Langreth, D. C. Van der Waals density functional: self-consistent potential and the nature of the van der Waals bond. *Phys. Rev. B: Condens. Matter Mater. Phys.* **2007**, *76*, 125112.
(101) Román-Pérez, G.; Soler, J. M. Efficient implementation of a van der Waals density functional: application to double-wall carbon nanotubes. *Phys. Rev. Lett.* **2009**, *103*, 096102.
(102) Larsen, A. H.; et al. The atomic simulation environment—a Python library for working with atoms. *J. Phys.: Condens. Matter* **2017**, *29*, 273002.
(103) Humphrey, W.; Dalke, A.; Schulten, K. VMD − Visual Molecular Dynamics. *J. Mol. Graphics* **1996**, *14*, 33−38.
(104) Vanderbilt, D. Soft self-consistent pseudopotentials in a generalized eigenvalue formalism. *Phys. Rev. B: Condens. Matter Mater. Phys.* **1990**, *41*, 7892−7895.
(105) Laasonen, K.; Car, R.; Lee, C.; Vanderbilt, D. Implementation of ultrasoft pseudopotentials in ab initio molecular dynamics. *Phys. Rev. B: Condens. Matter Mater. Phys.* **1991**, *43*, 6796−6799.
(106) Laasonen, K.; Pasquarello, A.; Car, R.; Lee, C.; Vanderbilt, D. Car-Parrinello molecular dynamics with Vanderbilt ultrasoft pseudopotentials. *Phys. Rev. B: Condens. Matter Mater. Phys.* **1993**, *47*, 10142−10153.
(107) Garrity, K. F.; Bennett, J. W.; Rabe, K. M.; Vanderbilt, D. Pseudopotentials for high-throughput DFT calculations. *Comput. Mater. Sci.* **2014**, *81*, 446−452.
(108) Monkhorst, H. J.; Pack, J. D. Special points for Brillouin-zone integrations. *Phys. Rev. B* **1976**, *13*, 5188−5192.